Kovove Mater. 64 2026 71–83
DOI: 10.31577/km.2026.2.71

Influence of Cu and C particle reinforcement on the mechanical, thermal, electrical, and soldering behavior of Sn88Bi12 solder alloy

Uroš Stamenković[1]*, Ivana Marković[1], Dragan Manasijević[1], Milan Gorgievski[1], Milan Nedeljković[1], Kristina Božinović[1], Avram Kovačević[1]

[1] *University of Belgrade, Technical faculty in Bor, Bor, Serbia*

Received 21 January 2026, received in revised form 17 March 2026, accepted 18 May 2026

Abstract

The development of low-temperature, lead-free solders with balanced mechanical reliability, functional properties, and soldering performance remains a key challenge in electronic packaging. This study systematically investigates the mechanical, electrical, thermal, microstructural, and soldering behavior of pure Sn, a hypoeutectic Sn88Bi12 alloy, and two Sn88Bi12-based composites reinforced with Cu and graphite particles. The addition of 12 wt.% Bi to pure Sn resulted in pronounced grain refinement and substantial increases in microhardness and tensile strength, while further improvements were achieved through particulate reinforcement. These strengthening effects were accompanied by moderate reductions in electrical conductivity and thermal transport properties due to enhanced electron and phonon scattering. Differential scanning calorimetry showed that Bi addition effectively lowers the melting temperature of Sn, whereas Cu and graphite reinforcements broaden the melting interval without increasing the melting temperature. Soldering tests on Cu substrates revealed improved wettability of Sn88Bi12 compared to pure Sn, characterized by a lower contact angle, enhanced spreading, and reduced intermetallic compound (IMC) thickness. Although particle reinforcement slightly reduced spreading behavior, both Cu and graphite effectively suppressed IMC growth, with graphite providing the strongest inhibition.

Key words: Sn88Bi12 alloy, Cu and C composites, thermophysical properties, mechanical properties, soldering behavior

1. Introduction

Microjoining of engineering materials is a critical process in modern industrial and manufacturing applications, particularly in electronics and microelectronic assembly. In microjoining technologies, metallic filler materials or intermediate layers, commonly referred to as solders, are employed to form reliable joints between components [1, 2]. Soldering materials play a fundamental role in the electronics industry by enabling stable electrical, thermal, mechanical, and physical connections in printed circuit boards (PCBs), electrical contacts, optoelectronic and photonic systems, and microelectronic devices. These materials provide the essential interface between electronic components and PCB substrates, thereby ensuring long-term functional reliability [3–7].

For nearly a century, the eutectic Sn-Pb solder has been widely utilized due to its favorable wettability, relatively low processing temperature, cost effectiveness, and reliable performance in electronic assemblies [8–12]. However, the presence of lead in solder alloys poses significant risks to human health and the environment. As a result, global regulatory initiatives have accelerated the transition toward lead-free solder materials. Since 2006, the European Union has mandated the use of lead-free solders in consumer electronics through the implementation of the WEEE and RoHS directives [13, 14]. In response to these restrictions, extensive research efforts have focused on the development and optimization of Pb-free solder alloys, investigating their mechanical, physical, and

*Corresponding author: e-mail address: ustamenkovic@tfbor.bg.ac.rs

corrosion-related properties across a wide range of binary, ternary, and multicomponent systems, including Sn-Cu, Sn-Ag, Sn-Ag-Cu, Sn-Zn, and Sn-Bi alloys [1, 8, 15, 16].

Among the various Pb-free alloy systems, eutectic Sn-58Bi has attracted considerable attention as a candidate for low-temperature soldering applications due to its low melting point of approximately 139 ℃ [17, 18]. Nevertheless, the high bismuth content in this eutectic composition is well known to induce brittleness, which limits its mechanical reliability in practical applications [8, 19]. To overcome this limitation, increasing research efforts have been directed toward hypoeutectic Sn-Bi alloys, in which the Bi content is reduced to achieve a more favorable balance between mechanical performance and melting behavior [10, 17, 20–23]. In these alloys, Bi does not form intermetallic compounds with Sn but exists either in solid solution or as a discrete secondary phase [17]. Reported improvements in hardness, tensile strength, and yield strength in these alloys have been attributed to mechanisms such as grain refinement, solid-solution strengthening, and precipitation effects, as demonstrated in previous studies [10, 12, 17, 20–23].

Despite these improvements, the addition of limited amounts of Bi to Sn-based alloys generally leads to only moderate enhancements in mechanical properties, primarily due to the intrinsic softness of the Sn matrix. To further improve performance, solder-based composite materials have been developed. As reported by M. B. K. T. Mekala et al. [1], composite systems can provide improved load-bearing capability and a more favorable balance between strength and ductility compared to monolithic solder alloys. Consequently, various reinforcement strategies have been explored for Sn-Bi solders, including the incorporation of Al_2O_3 [24], $BaTiO_3$ [25], Sb_2O_3 [20], carbon nanotubes [26], and graphene nanosheets [23]. Ceramic and carbon-based reinforcements are particularly attractive due to their high strength and chemical stability, which can contribute to grain refinement, intermetallic compound (IMC) modification, and improved microstructural uniformity. Several studies have also reported enhanced solder wettability on metallic substrates, manifested by reduced contact angles, following the incorporation of nanoscale reinforcements [1, 8]. Overall, these approaches aim to enhance mechanical, physical, and structural properties, as well as soldering performance on Cu substrates, while maintaining or reducing the melting temperature of the solder material.

A critical review of the existing literature reveals that, in comparison to mechanical and microstructural investigations, studies addressing the thermal properties (such as thermal diffusivity and conductivity) and electrical characteristics (including electrical resistivity and conductivity) of Sn-Bi alloys and their composite counterparts remain relatively limited. In this context, the present study systematically investigates the mechanical, electrical, thermal, and structural behavior, along with the soldering performance, of a hypoeutectic Sn88Bi12 alloy and two composite systems, Sn88Bi12 + Cu and Sn88Bi12 + C. The obtained results are further compared with those of pure Sn to provide a comprehensive and comparative evaluation of the developed solder materials.

The experimental procedures employed in this work were designed to ensure reproducibility and consistency across all investigated materials. Details regarding alloy preparation, composite fabrication, characterization techniques, and soldering performance evaluation are described in the following section.

2. Experimental Procedure

2.1. Alloy and composite preparation

Pure Sn and a hypoeutectic Sn88Bi12 alloy were prepared using high-purity tin (99.95 %) and bismuth (99.9 %) by the stir-casting method. The constituent metals were charged into a graphite crucible and melted in an electric resistance furnace at 350 ℃. After complete melting, the liquid alloy was mechanically stirred using a graphite stirrer to promote chemical homogeneity. The melt was stirred for 10 s and subsequently cast into a cylindrical steel mold with a diameter of 13 mm and a length of 100 mm.

Two composite materials were produced using the same base alloy preparation procedure with an additional reinforcement incorporation step. The Sn88Bi12 alloy was reinforced separately with 0.2 wt.% graphite powder (particle size $\leq$ 45 μm) and 0.2 wt.% atomized copper powder (particle size $\leq$ 45 μm), producing Sn88Bi12 + C and Sn88Bi12 + Cu composites, respectively. The reinforcement particles were introduced directly into the molten alloy during mechanical stirring to facilitate their entrainment into the melt and promote dispersion within the matrix.

For the preparation of the graphite-reinforced composite, slight adjustments to the processing parameters were implemented to improve the incorporation of low-density graphite particles. In particular, the melt temperature and stirring conditions (stirring speed and stirrer orientation) were carefully adjusted to enhance particle entrainment and minimize flotation during processing. After stirring for approximately 30 s, the composite melts were cast into the same steel mold geometry as used for the monolithic alloy.

2.2. Heat treatment of the ingots

All cast ingots – pure Sn, Sn88Bi12 alloy, and both composite variants were subjected to homogenization heat treatment at 200 ℃ for 20 h in order to improve chemical and microstructural homogeneity.

2.3. Sample sectioning

Following homogenization, the ingots were sectioned using a Struers Mesotom precision cutter. The resulting specimens were prepared according to the requirements of the respective characterization techniques.

2.4. Mechanical property evaluation

2.4.1. Microhardness testing

Vickers microhardness measurements were performed in accordance with ASTM E384 [27] using a PMT-3 microhardness tester, applying a load of 0.5 N and a dwell time of 15 s. Prior to testing, samples were ground and polished to a mirror finish. For each sample, 5–7 indentations were made at different locations, and the average value was reported.

2.4.2. Tensile testing

Tensile specimens in the form of wires with a diameter of 5 mm were prepared from the homogenized ingots. The initial ingot diameter of 13 mm was reduced to 5 mm by cold rolling using a Joliot rolling mill. The rolled wires were subsequently annealed to eliminate strain hardening and ensure a fully recrystallized microstructure. Tensile tests were conducted using a Mohr-Federhaff-Losenhausen universal testing machine, and the tensile properties were recorded.

2.5. Thermophysical and electrical properties

2.5.1. Electrical conductivity:

Electrical conductivity measurements were carried out at room temperature using a Foerster Sigmatest 2.063 conductivity tester. Multiple measurements were performed for each sample, and the reported value represents the average.

2.5.2. Thermal diffusivity, specific heat capacity, and thermal conductivity

Thermal diffusivity and specific heat capacity were determined using the light flash method over a temperature range of 25–100 ℃ with a TA Instruments *DXF-500* apparatus. In this method, the lower surface of a plane-parallel specimen is heated by a short xenon flash pulse, while the resulting temperature rise on the upper surface is recorded by an infrared detector. Thermal diffusivity is calculated from the transient temperature response. At each temperature interval, three measurements were performed, and the average value was used.

Thermal conductivity (λ) was subsequently calculated using Eq. (1):

$$\lambda = \alpha \times \rho \times C_{\mathrm{p}}, \quad (1)$$

where λ is the thermal conductivity ($\mathrm{W\,m^{-1}\,K^{-1}}$), α is the thermal diffusivity ($\mathrm{m^2\,s^{-1}}$), ρ is the density ($\mathrm{kg\,m^{-3}}$), and C_{p} is the specific heat capacity ($\mathrm{J\,g^{-1}\,K^{-1}}$).

2.5.3. Differential scanning calorimetry (DSC)

Melting behavior was analyzed using a TA Instruments SDT Q600 differential scanning calorimeter. Samples with a mass of approximately 20 mg were heated from room temperature to 300 ℃ at a heating rate of 10 ℃ $\mathrm{min^{-1}}$ under a nitrogen atmosphere.

2.6. Microstructural characterization

Microstructural and compositional analyses were conducted using a Tescan Vega 3 LMU scanning electron microscope (SEM) equipped with an Oxford Instruments X-act energy-dispersive spectroscopy (EDS) detector. This setup enabled phase identification and spatial distribution analysis of the reinforcement particles. Prior to examination, samples were wet-ground, polished, and chemically etched using a solution composed of 2 ml HCl and 2 ml HNO_3 in 96 ml ethanol.

2.7. Soldering characteristics

Soldering behavior was evaluated through measurements of the wetting (contact) angle, spreading area, spreading ratio, and intermetallic compound (IMC) layer thickness.

Copper substrates with dimensions of 20 × 20 × 0.5 $\mathrm{mm^3}$ were ground using SiC abrasive papers and polished with alumina slurry to achieve a mirror finish. The substrates were then cleaned in a 10% H_2SO_4 solution to remove surface oxides, rinsed sequentially with acetone and ethanol, and dried with warm air. Cylindrical solder specimens with a diameter of 2 mm and a height of 2 mm were prepared from each alloy and composite. RMA218 flux was applied at the center of the substrate together with the solder specimen.

2.7.1. Spreading area

The spreading area was determined by photographing the reflowed solder using a digital camera and analyzing the images with *ImageJ software.*

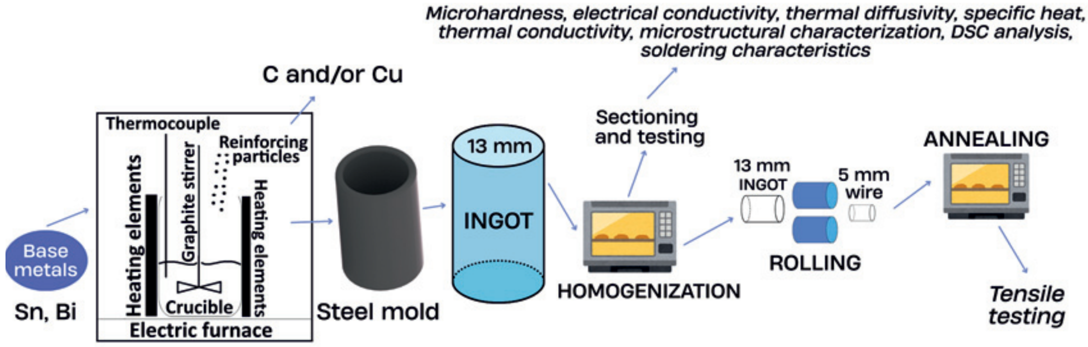

Fig. 1. Overview of the manufacturing process of alloys and composites, and sample sectioning for analysis.

2.7.2. *Spreading ratio*

The spreading ratio (SR) was calculated using Eq. (2):

$$\mathrm{SR}(\%) = ((D - H)/D) \times 100, \quad (2)$$

where D is the equivalent diameter of the solder assuming a spherical geometry ($D = 1.24V^{1/3}$), V is the solder volume determined from mass and density, and H is the height of the solder after reflow.

2.7.3. *Contact angle and IMC thickness*

Prior to the measurement of contact angles and intermetallic compound (IMC) layer thicknesses, the Cu substrates with solidified solder joints were precision cut, embedded in epoxy resin, and allowed to cure. The cross-sectioned samples were subsequently prepared following the same metallographic procedure used for SEM/EDS analysis, including grinding and polishing to obtain a deformation-free surface. After preparation, the samples were examined and imaged using Carl Zeiss Jena Epytip 2 and Reichert MeF2 optical microscopes. Contact angles and IMC layer thicknesses were then quantified using *ImageJ software* based on the acquired micrographs.

A schematic overview of the alloy and composite fabrication process, as well as sample sectioning for subsequent characterization, is presented in Fig. 1.

3. Results and Discussion

3.1. *Mechanical properties*

Mechanical properties are among the most critical characteristics of solder materials, as solder joints are required to withstand mechanical loading and deformation during service. In this study, the mechanical performance of pure Sn, the Sn88Bi12 alloy, and Sn88Bi12-based composites reinforced with Cu or C particles was evaluated through microhardness and tensile strength measurements.

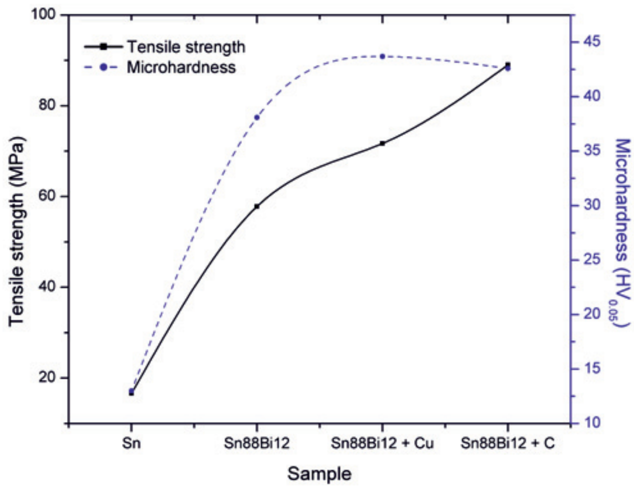

Fig. 2. The change in tensile strength and microhardness of the investigated samples.

Figure 2 presents the variation in microhardness and ultimate tensile strength (UTS) for the investigated materials. Microhardness is an important parameter for solder joints, as they may be subjected to localized stresses, wear, and mechanical damage during service [28]. As shown in Fig. 2, pure tin exhibits the lowest microhardness value, measured at 13 HV0.05. This result is in good agreement with literature data, where pure Sn is reported to possess a Vickers hardness of approximately 10–15 HV, reflecting its inherently soft and ductile nature under low-load indentation [17, 21].

The addition of 12 wt.% Bi to pure Sn leads to a pronounced increase in microhardness, from 13 to 38 HV0.05. This significant improvement can be attributed primarily to microstructural refinement and solid-solution/second-phase strengthening effects associated with Bi addition. Bismuth promotes refinement of the β-Sn grain structure, resulting in reduced

Table 1. The change in electrical conductivity of investigated samples

Sample	Electrical conductivity (MS m^{-1})
Pure Sn	7.7
Sn88Bi12	5.73
Sn88Bi12 + Cu	5.6
Sn88Bi12 + C	5.4

grain size and an increased density of grain boundaries. According to the Hall-Petch relationship, this grain refinement effectively impedes dislocation motion, thereby enhancing hardness and strength. Similar increases in hardness with Bi addition to Sn-based alloys have been widely reported in the literature [12, 21, 22].

Further enhancement in microhardness is observed upon reinforcing the Sn88Bi12 alloy with Cu or C particles. The microhardness increases to 43.7 HV0.05 for the Cu-reinforced composite and 42.6 HV0.05 for the C-reinforced composite. This additional improvement is attributed to dispersion strengthening, arising from the relatively homogeneous distribution of reinforcement particles within the Sn-Bi matrix. These particles act as obstacles to dislocation motion and contribute to increased resistance to localized plastic deformation. The strengthening effect of particulate reinforcements in Sn-Bi and other Sn-based solder alloys has been well documented in previous studies [7].

Tensile properties are of paramount importance for solder materials, as insufficient mechanical strength can lead to premature joint failure during service. The observed trends in tensile strength closely follow those obtained for microhardness. The UTS increases markedly with Bi addition, rising from 16.6 MPa for pure Sn to 57.8 MPa for the Sn88Bi12 alloy. This substantial improvement reflects the combined effects of grain refinement and Bi-induced strengthening mechanisms discussed above.

An even more pronounced strengthening effect is achieved with the addition of reinforcement particles. The UTS increases further to 71.7 MPa for the Sn88Bi12 + Cu composite and to 89 MPa for the Sn88Bi12 + C composite. Compared with the microhardness results, the influence of reinforcement particles on tensile strength is more significant, indicating their effective role in restricting plastic deformation and delaying crack initiation and propagation under tensile loading. Similar enhancements in tensile strength due to particulate or nanoscale reinforcements in Sn-based solder alloys have been reported in the literature [7, 8, 17, 23, 29].

3.2. Electrical and thermal properties

Since one of the primary functions of a solder joint is to transmit electrical power or signals between joined components, the electrical conductivity of the solder material is a critical property. Table 1 summarizes the electrical conductivity values of pure Sn, the Sn88Bi12 alloy, and the corresponding Cu- and C-reinforced composites measured at room temperature.

As evident from the data, the addition of Bi leads to a pronounced reduction in electrical conductivity compared with pure Sn. This decrease can be attributed to several concurrent mechanisms. Bismuth possesses a significantly lower intrinsic electrical conductivity than tin, and its incorporation into the Sn matrix results in the formation of Bi-rich phases with inferior charge transport capability. In addition, the atomic size mismatch between Sn and Bi induces lattice distortion, while the multiphase microstructure and refined grain structure introduce a high density of phase and grain boundaries. These microstructural features act as effective electron scattering centers, reducing the electron mean free path and increasing electrical resistivity in accordance with Matthiessen's rule [30]. Similar increases in electrical resistivity with Bi addition to Sn-based alloys have been reported in the literature [13, 31, 32].

A further, albeit less pronounced, decrease in electrical conductivity is observed upon reinforcing the Sn88Bi12 alloy with Cu or C particles. The electrical conductivity decreases to 5.6 MS m^{-1} for the Cu-reinforced composite and to 5.4 MS m^{-1} for the C-reinforced composite. This reduction is attributed to the presence of reinforcement particles within the Sn-Bi matrix, which act as additional electron scattering sites and disrupt continuous conductive pathways. While some studies report that nanoscale reinforcements may have a negligible or even beneficial effect on the electrical conductivity of lead-free composite solders [33, 34], other investigations have shown that micron-sized particles tend to reduce electrical conductivity, consistent with the behavior observed in the present study [35].

Thermal diffusivity is a key parameter for evaluating heat dissipation in solder joints, as it directly governs the thermal conductivity and thus the overall thermal management capability of electronic interconnections [36]. Figures 3 and 4 present the variation of thermal diffusivity and thermal conductivity, respectively, for pure Sn, the Sn88Bi12 alloy, and the corresponding Cu- and C-reinforced composites over the temperature range of 25–100 °C.

As shown in the figures, the Sn88Bi12 alloy and both investigated composites exhibit lower thermal diffusivity and thermal conductivity compared to pure tin across the entire temperature range. In metallic and alloy systems, heat transfer is primarily mediated by free electrons and lattice vibrations (phonons), and the total thermal conductivity reflects the com-

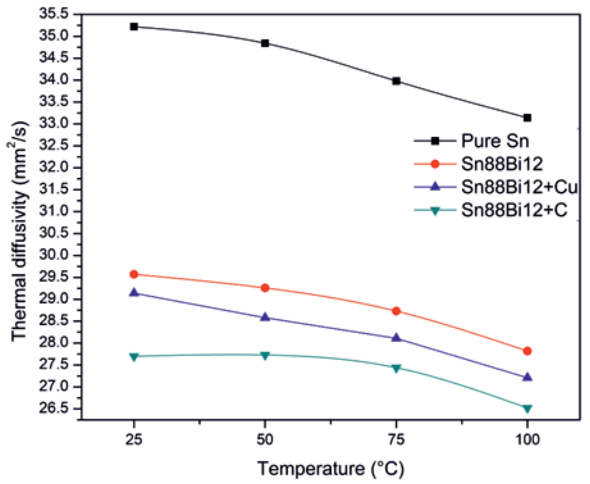

Fig. 3. The change in thermal diffusivity of the investigated samples.

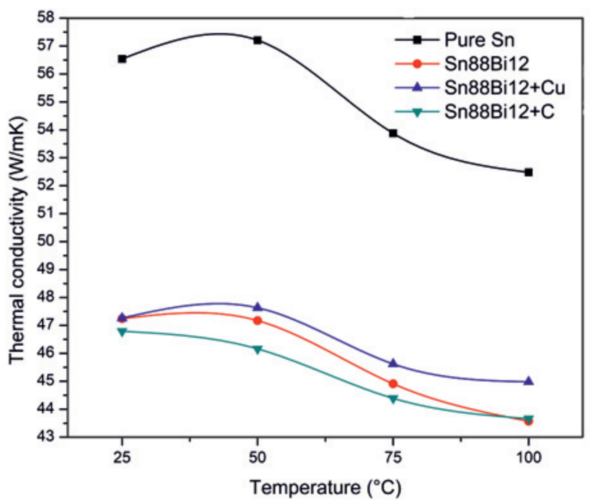

Fig. 4. The change in thermal conductivity of the investigated samples.

bined contributions of these two carriers. Similar to the trends observed for electrical conductivity, the incorporation of Bi and reinforcing particles (Cu or C) enhances electron and phonon scattering, leading to a reduction in both thermal diffusivity and thermal conductivity. Although Bi addition reduces the free-electron concentration and thereby increases the relative contribution of phonons to heat transport, phonon-mediated thermal conductivity in Sn-Bi alloys remains strongly limited by lattice distortion, grain refinement, and the presence of phase boundaries. As a consequence, increasing Bi content results in a net decrease in thermal conductivity and thermal diffusivity [37].

Regarding the influence of reinforcing particles, previous studies have reported both positive and negative effects of particle additions on the thermal properties of solder matrices, depending on particle type, size, distribution, and intrinsic thermal conductivity [38, 39]. In the present work, the composite containing Cu particles exhibit thermal conductivity values comparable to, or only slightly higher than, those of the unreinforced Sn88Bi12 alloy. This behavior can be attributed to the inherently high thermal conductivity of copper, which partially compensates for the increased scattering of electrons and phonons, particularly at elevated temperatures. Notably, this compensating effect becomes more evident at 100 ℃ and is not reflected in room-temperature electrical conductivity measurements, highlighting the different temperature sensitivities of thermal and electrical transport mechanisms.

The influence of temperature on thermal diffusivity and thermal conductivity is evident for all investigated samples. With increasing temperature, enhanced lattice vibrations and intensified scattering processes reduce the mean free paths of heat carriers in pure metals, alloys, and the investigated composites. Consequently, a progressive decrease in both thermal diffusivity and thermal conductivity with temperature is observed for all materials. [40, 41].

3.3. Microstructural analysis

Figure 5 presents SEM micrographs of the investigated materials. The microstructure of pure Sn, shown in Fig. 5a, is characterized by relatively large β-Sn grains, which is typical for cast and homogenized tin. The addition of Bi leads to a pronounced refinement of the Sn grain structure, as observed in the Sn88Bi12 alloy (Fig. 5b). In this alloy, Bi-rich phases, appearing as bright regions in backscattered electron images, are predominantly located along Sn grain boundaries, consistent with the limited solubility of Bi in β-Sn and its tendency to segregate and precipitate during solidification and subsequent homogenization treatment.

Further microstructural refinement is observed in the Sn88Bi12 + Cu composite (Fig. 5c). The presence of copper promotes additional grain refinement of both the Sn matrix and the Bi-rich phase. Discrete Cu-containing particles are not observed as unreacted metallic Cu, indicating that the added Cu powder reacted with the molten Sn-based matrix during casting and/or subsequent homogenization heat treatment. At higher magnification, Cu-containing phases embedded within the Sn-rich matrix become evident and were subsequently identified by EDS analysis.

In contrast, the Sn88Bi12 + C composite (Fig. 5d) exhibits dark, irregular regions corresponding to graphite particles. These carbon-rich phases appear as partially dispersed blocky agglomerates rather than uniformly distributed fine particles. This morphology reflects the poor wettability of graphite by molten

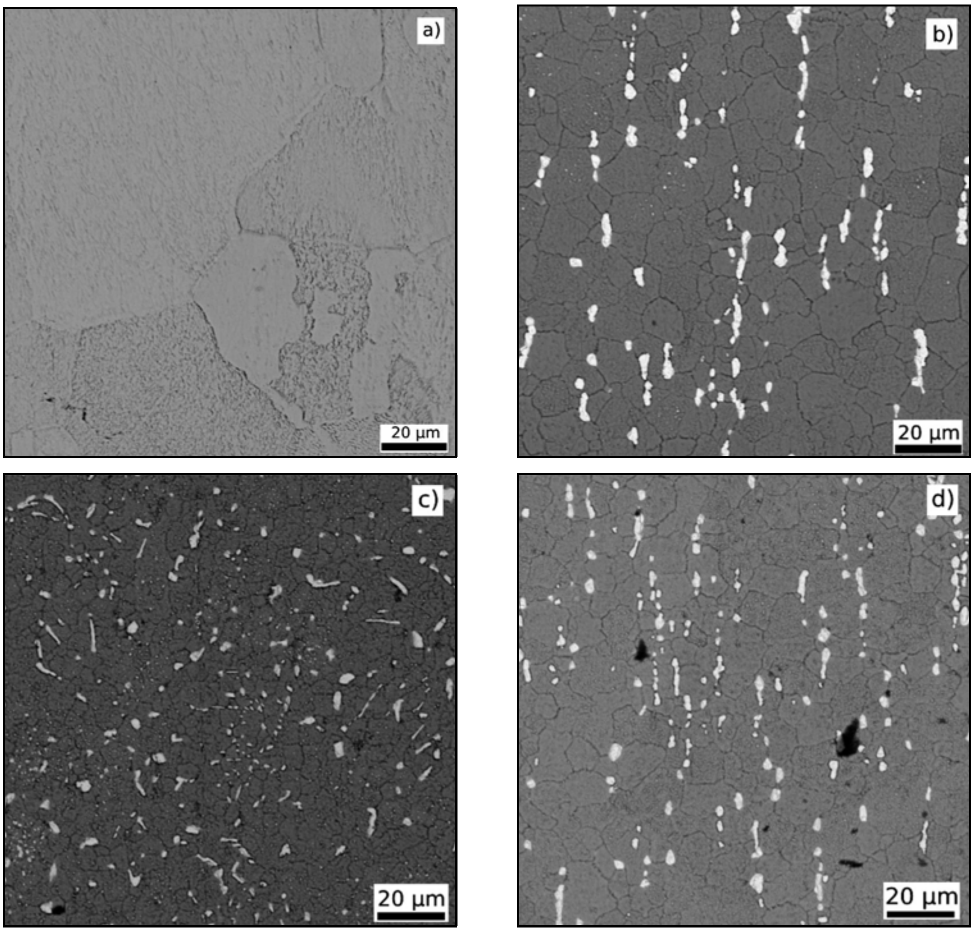

Fig. 5. SEM microphotographs for: (a) pure Sn, (b) Sn88Bi12, (c) Sn88Bi12 + Cu, and (d) Sn88Bi12 + C.

Sn-based alloys and the difficulty of achieving homogeneous dispersion of carbonaceous reinforcements, even under mechanical stirring conditions.

Figure 6 with corresponding tables show SEM-EDS analyses of the Sn88Bi12 alloy and the two investigated composites. For the Sn88Bi12 alloy (Fig. 6a), EDS spectra confirm a Sn-rich matrix (spectrum S3) with Bi-rich phases (spectra S1 and S2) decorating the grain boundaries. The presence and morphology of Bi-rich phases within the Sn matrix are in good agreement with previous reports on Sn-Bi solder alloys [17, 21, 22, 29].

SEM-EDS analysis of the Sn88Bi12 + Cu composite reveals discrete Cu-enriched regions embedded within the Sn-rich matrix (spectra S1 and S3). Point analyses demonstrate a clear enrichment of Cu relative to the surrounding matrix, confirming that the Cu reinforcement does not remain inert during processing. Based on the observed morphology, elemental distribution, and the strong thermodynamic affinity between Cu and Sn, these Cu-containing phases are attributed to the formation of Cu-Sn intermetallic compounds, most commonly Cu_6Sn_5, as widely reported for Sn-based composite solders reinforced with Cu particles [18].

For the Sn88Bi12 + C composite, EDS analysis (spectra S1 and S3) confirms the presence of carbon within the microstructure. The graphite particles appear as dark, blocky regions that are only partially dispersed throughout the Sn–Bi matrix, indicating limited interfacial bonding between graphite and the molten solder. Unlike metallic reinforcements, graphite does not chemically react with the Sn-Bi matrix and therefore remains as a discrete, inert phase. The observed agglomeration and non-uniform distribution of graphite particles are commonly reported for Sn-based solder composites reinforced with carbonaceous materials and can significantly influence mechanical strengthening, as well as electrical and thermal transport properties, through localized stress concentrations and enhanced electron and phonon scattering [33].

Overall, the SEM and EDS observations are fully consistent with the trends observed in the mechanical, thermal, and electrical characterization of the investigated materials.

3.4. Melting behavior

The melting temperature is a critical characteristic

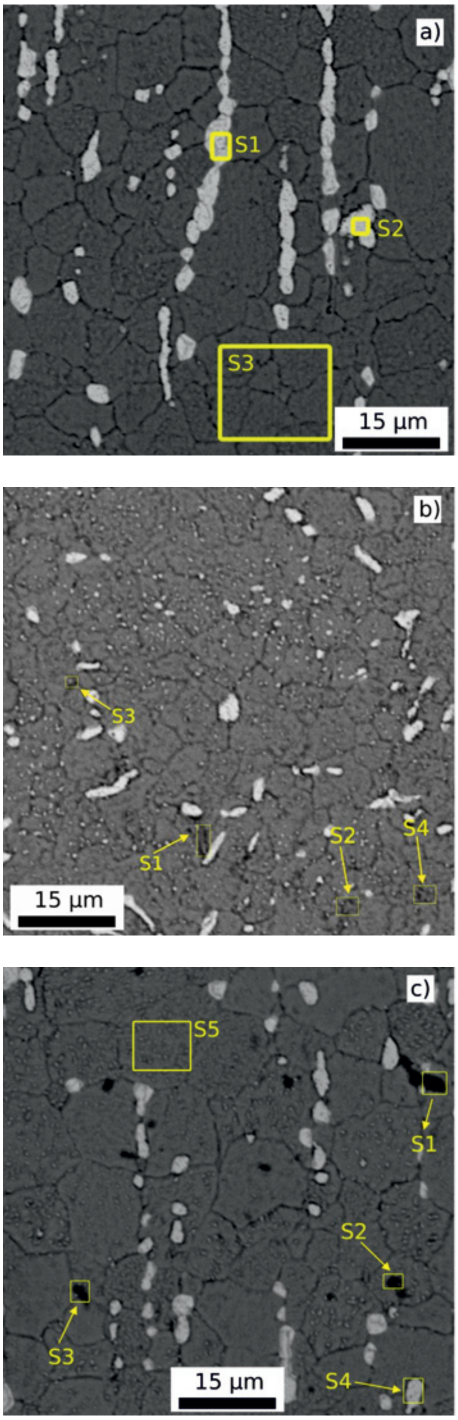

Spectrum	Sn	Bi
S1	/	100.00
S2	/	100.00
S3	97.22	2.78

**results are given in atomic %*

Spectrum	Cu	Sn	Bi
S1	8.18	89.20	2.62
S2	/	96.97	3.03
S3	19.22	80.78	/
S4	/	96.82	3.18

**results are given in atomic %*

Spectrum	C	Sn	Bi
S1	87.12	12.45	0.43
S2	79.60	19.92	0.49
S3	71.20	28.16	0.65
S4	/	4.44	95.56
S5	/	95.65	4.45

**results are given in atomic %*

Fig. 6. EDS analysis of SEM microphotographs for: (a) Sn88Bi12, (b) Sn88Bi12 + Cu, and (c) Sn88Bi12 + C.

of solder materials, as an ideal solder should exhibit a low melting temperature and a narrow melting interval [10]. Ideally, maintaining a processing temperature below 250 ℃ helps prevent damage to adjacent components while preserving the structural integrity of the solder joint [42]. Differential scanning calorimetry (DSC) was employed to evaluate the melting behavior of the investigated samples. Measurements were conducted under an inert argon atmosphere over a temperature range of 30–300 ℃, and the resulting DSC curves were analyzed.

Figure 7 presents the DSC heating curves of pure Sn, the Sn88Bi12 alloy, and the corresponding Sn88Bi12 + Cu and Sn88Bi12 + C composites. The onset and offset temperatures extracted from the DSC curves are summarized in Table 2 and were used to evaluate the solidus-liquidus behavior and melting intervals of the investigated materials.

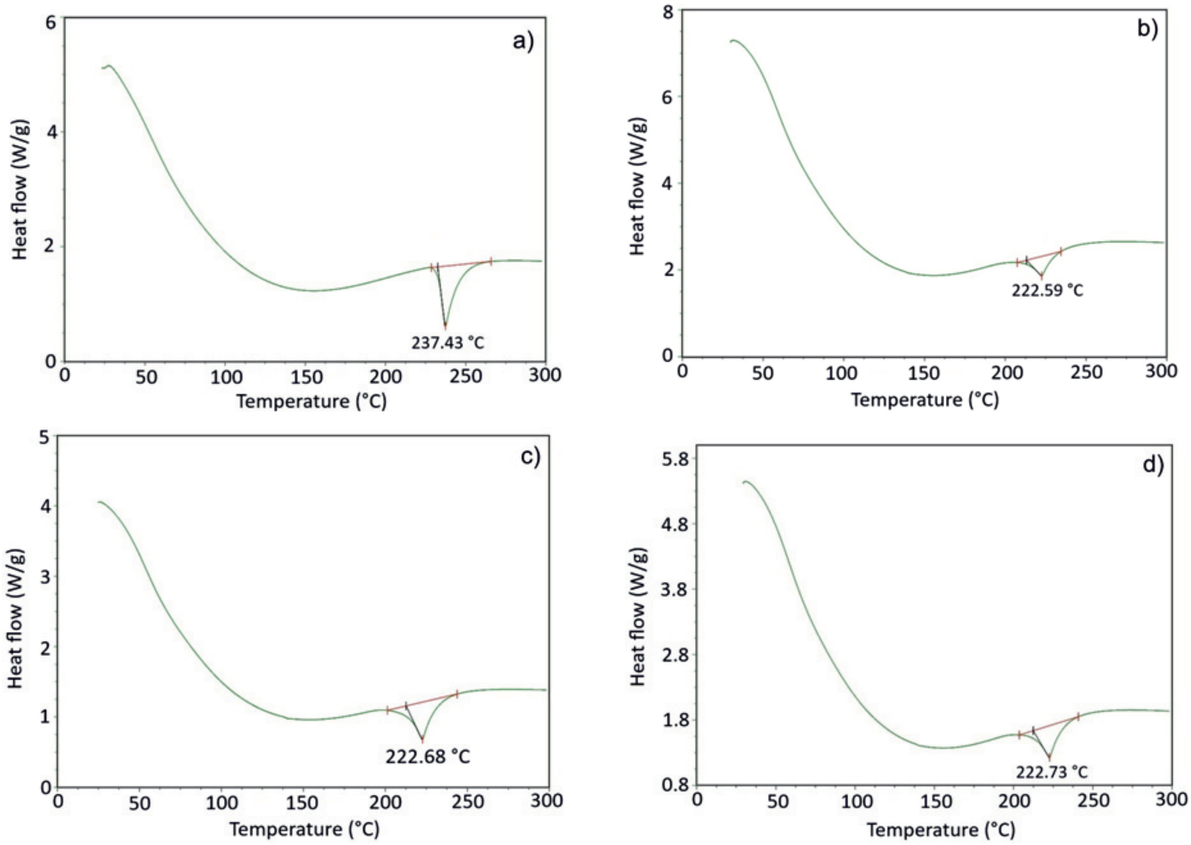

Fig. 7. DSC heating curves for: (a) pure Sn, (b) Sn88Bi12, (c) Sn88Bi12 + Cu, and (d) Sn88Bi12 + C.

Table 2. DSC curve analysis of the investigated samples

Sample	T_{onset} (℃)	T_{offset} (℃)	Melting range (℃)
Pure Sn	228.7	258.8	30.1
Sn88Bi12	207.5	233.9	26.4
Sn88Bi12 + Cu	201.1	243.5	42.4
Sn88Bi12 + C	204.1	241.3	37.2

Pure Sn exhibits an onset temperature of 228.7 ℃ and an offset temperature of 258.8 ℃, corresponding to a relatively wide melting interval of approximately 30 ℃. This broad melting range can be attributed to thermal lag and kinetic effects associated with the applied heating rate, which commonly lead to delayed completion of melting in pure metals during DSC measurements.

The addition of 12 wt.% Bi significantly reduces both the onset and offset temperatures, which decrease to 207.5 and 233.9 ℃, respectively, for the Sn88Bi12 alloy. This behavior is consistent with the Sn-Bi phase diagram and confirms the effectiveness of Bi in lowering the solidus and liquidus temperatures of Sn-based solders. The reduced melting interval of the Sn88Bi12 alloy compared to pure Sn indicates a more well-defined melting behavior, which can be attributed to the lowering of the solidus temperature and the presence of Bi-rich phases that initiate localized melting at lower temperatures. This behavior is beneficial for low-temperature soldering applications. Several authors have investigated the melting characteristics of Sn-Bi solder alloys using DSC analysis. Y. A. Shen et al. [17] reported melting temperatures of approximately 226 ℃ and 210 ℃ for Sn-2.5Bi and Sn-5Bi alloys, respectively. Similarly, W. Firdaus et al. [43] measured melting temperatures of approximately 232 ℃ for pure Sn, 227 ℃ for Sn-3Bi, and 208 ℃ for Sn-21Bi alloys. Y. Li et al. [10] reported a melting temperature of approximately 208 ℃ for the Sn-15Bi alloy.

Further modification of the Sn88Bi12 alloy by the addition of Cu or C particles leads to additional changes in the melting behavior. The Sn88Bi12 + Cu composite exhibits a further reduction in onset temperature to 201.1 ℃, while the offset temperature increases to 243.5 ℃, resulting in a substantially wider melting interval of approximately 42 ℃. S. N. Alam et al. suggested that addition of Cu can widen the melting interval when added to the eutectic Sn-Bi alloy [44]. A similar trend is observed for the Sn88Bi12 + C composite, with an onset temperature of 204.1 ℃

Table 3. Soldering characteristics of the investigated samples

Sample	Contact angle (°)	Spreading area (mm^2)	Spreading ratio (%)	IMC layer thickness (μm)
Pure Sn	23.27	23.77	78.23	2.84
Sn88Bi12	18.35	24.27	79.29	2.38
Sn88Bi12 + Cu	25.12	21.11	75.36	2.47
Sn88Bi12 + C	24.8	21.73	75.57	2.25

and an offset temperature of 241.3 ℃. The lowered onset temperatures suggest facilitated initiation of melting, likely promoted by heterogeneous nucleation effects and local compositional variations near the particle-matrix interfaces. In contrast, the elevated offset temperatures indicate delayed completion of melting, which may be attributed to increased thermal and microstructural heterogeneity, as well as possible interfacial reactions in the case of Cu-containing composites.

Overall, the DSC results demonstrate that Bi addition effectively lowers the melting temperature of Sn-based solders, while the incorporation of Cu or C reinforcing particles broadens the melting interval without increasing the melting temperature. The widening of the melting interval has been reported for other Sn-based composite solders and reflects the complex heat-transfer behavior and phase-interaction processes introduced by particulate reinforcements [23, 45]. Although a broader melting range requires more careful control of reflow conditions, it does not negate the advantages of composite solders, particularly when accompanied by improvements in mechanical performance.

3.5. Soldering performance on Cu substrates

Soldering performance is a critical parameter for the evaluation of low-temperature solder alloys, as the integrity and reliability of the joint formed between the solder and the substrate are governed by the soldering process and the intrinsic properties of the solder material. The soldering performance can be assessed through key parameters such as wettability, spreading area, and spreading ratio, as well as through the characterization of interfacial reactions between the solder and the substrate, typically quantified by measuring the thickness of the formed intermetallic compound (IMC) layer [1, 8, 17].

Table 3 summarizes the measured values of contact angle, spreading area, spreading ratio, and intermetallic compound (IMC) layer thickness for pure Sn, the Sn88Bi12 alloy, and the two investigated Sn88Bi12-based composites. Among the examined materials, pure Sn exhibits the highest contact angle and the thickest IMC layer, indicating inferior soldering performance despite its relatively large spreading area. This behavior is consistent with the known limitations of pure tin, which generally exhibits less favorable wetting kinetics and enhanced interfacial reactivity with Cu substrates.

The addition of Bi to the Sn matrix leads to a clear improvement in soldering performance. The Sn88Bi12 alloy exhibits the lowest contact angle, the largest spreading area, and a reduced IMC thickness compared to pure Sn. This enhanced wettability can be attributed primarily to the reduction in liquidus temperature of the Sn-Bi alloy, which increases molten solder fluidity at the soldering temperature of 250 ℃ and facilitates improved spreading on the Cu surface. In addition, Bi is known to segregate at the Sn/Cu interface and act as a diffusion barrier, thereby suppressing excessive interdiffusion between Sn and Cu and limiting IMC growth [11, 17].

Further modification of the Sn88Bi12 alloy by the addition of Cu particles results in a deterioration of soldering behavior. The Sn88Bi12 + Cu composite exhibits the highest contact angle among all investigated samples, accompanied by reduced spreading area and spreading ratio, as well as a slight increase in IMC thickness relative to the Sn88Bi12 alloy. This behavior is associated with the formation of Sn-Cu intermetallic compounds during melting and homogenization, which increase the effective viscosity of the molten solder and restrict its spreading capability [18]. Moreover, DSC analysis (Table 2) revealed that this composite exhibits the broadest melting interval, indicating delayed and non-uniform melting at the soldering temperature. The prolonged presence of partially molten regions, combined with pre-existing Sn-Cu intermetallics, promotes sustained interfacial reactions and contributes to increased IMC growth.

The Sn88Bi12 + C composite exhibits spreading behavior comparable to that of the Cu-reinforced composite, with similarly increased contact angle and reduced spreading area and spreading ratio relative to the unreinforced Sn88Bi12 alloy. Notably, this composite shows the thinnest IMC layer among all investigated materials. Graphite is chemically inert with respect to the molten Sn-Bi matrix and exhibits poor wettability, resulting in limited interaction with the substrate during soldering. The presence of graphite particles at or near the solder/substrate interface can act as a physical barrier to atomic diffusion and grain boundary migration, thereby effectively inhibiting IMC growth.

Overall, the observed soldering behavior reflects the combined effects of alloy composition, melting characteristics, and the presence of reinforcing particles, and is consistent with the trends identified in the DSC, microstructural, mechanical, thermal, and electrical characterizations.

4. Conclusions

In this study, the mechanical, thermal, electrical, microstructural, and soldering performance of pure Sn, a hypoeutectic Sn88Bi12 alloy, and two Sn88Bi12-based composites reinforced with Cu and graphite particles were systematically investigated. Based on the obtained results, the following conclusions can be drawn:

1. The addition of 12 wt.% Bi to pure Sn resulted in pronounced microstructural refinement and substantial improvement in mechanical properties. The microhardness and tensile strength increased by approximately 192 and 248 %, respectively. Further reinforcement of the Sn88Bi12 alloy with Cu particles led to additional increases in microhardness and tensile strength of about 15 and 24 %, respectively, relative to the alloy matrix. Graphite reinforcement also enhanced mechanical performance, increasing microhardness by approximately 12 % and tensile strength by as much as 54 %.

2. Electrical conductivity decreased by approximately 25.6 % upon the addition of 12 wt.% Bi to pure Sn. Further reductions were observed in the composite systems, amounting to 2.27 % for Cu reinforcement and 5.76 % for graphite reinforcement relative to the Sn88Bi12 alloy. At room temperature, thermal diffusivity and thermal conductivity decreased by approximately 16.0 and 16.4 %, respectively, with Bi addition. Cu reinforcement caused only a minor reduction in thermal diffusivity (about 1.45 %) while maintaining or slightly increasing thermal conductivity at elevated temperatures, whereas graphite reinforcement led to reductions of approximately 6.32 % in thermal diffusivity and 0.95 % in thermal conductivity.

3. DSC analysis confirmed that Bi addition effectively lowers the onset melting temperature of Sn-based solders, while the incorporation of Cu or graphite particles broadens the melting interval without increasing the melting temperature, preserving suitability for low-temperature soldering applications.

4. SEM-EDS analysis revealed clear microstructural refinement with alloying and reinforcement. Compared to pure Sn, the addition of Bi led to pronounced grain refinement, which was further enhanced by the incorporation of Cu particles into the Sn88Bi12 matrix. SEM-EDS analysis also showed that Cu particles do not remain inert within the Sn88Bi12 alloy but react with molten Sn to form Cu-containing intermetallic phases, most likely Cu_6Sn_6. In contrast, graphite remains chemically inert, appearing as a discrete phase with limited wettability and partial agglomeration within the solder matrix.

5. Soldering performance evaluation demonstrated that the Sn88Bi12 alloy exhibited the best wettability among the investigated materials, characterized by a reduced contact angle, increased spreading area, and a thinner intermetallic compound (IMC) layer compared to pure Sn.

6. The addition of Cu and graphite reinforcements resulted in increased contact angles and reduced spreading behavior due to restricted melt flow and interfacial effects. Nevertheless, both composites exhibited thinner IMC layers than pure Sn, with the Sn88Bi12 + C composite showing the lowest IMC thickness.

Overall, the results demonstrate that hypoeutectic Sn88Bi12 and its composite variants represent a viable pathway toward low-temperature, lead-free solder systems with tunable performance. Importantly, the substantial percentage increases in mechanical properties far outweigh the relatively modest percentage decreases in electrical and thermal transport properties, highlighting a favorable performance trade-off. In particular, graphite reinforcement is effective in suppressing IMC growth, while Cu reinforcement contributes to microstructural stability, making these materials promising candidates for specialized electronic packaging applications.

Acknowledgement

This work was supported by Ministry of Science, Technological Development and Innovation of the Republic of Serbia, with the funding of the scientific research work at the University of Belgrade, Technical Faculty in Bor, according to the contract with registration number 451-03-34/2026-03/200131.

References

[1] M. B. K. T. Mekala, A. Sharma, S. Das, K. Das, A review on nanodispersed lead-free solders in electronics: synthesis, microstructure and intermetallic growth characteristics, J. Mater. Sci. 57 (2022) 8597–8633. https://doi.org/10.1007/s10853-022-07187-8

[2] K. J. Puttlitz, K. A. Stalter, Handbook of lead-free solder technology for microelectronic assemblies. Marcel Dekker, Inc., New York (2004). ISBN: 9780824748708.

[3] E. R. Arriola, J. Xie, M. A. M. Ibrahim, C. Wang, C. Hu, Wafer-level chip-scale package lead-free solder fatigue: A critical review, Eng. Fail. Anal. 144 (2023) 106986. https://doi.org/10.1016/j.engfailanal.2022.106986

[4] R. Mahmudi, A. Maraghi, A. R. Geranmayeh, High-temperature shear strength and hardness of cast

lead-free solders, Kovove Mater. 55 (2017) 211–216. https://doi.org/10.4149/km_2017_3_211
[5] L. Zhang, S. Xue, L. Gao, G. Zeng, Y. Chen, S. Yu, Z. Sheng, Creep behavior of SnAgCu solders with rare earth Ce doping, Trans. Nonferrous Met. Soc. China 20 (2010) 412–417. https://doi.org/10.1016/S1003-6326(09)60155-2
[6] A. A. El-Daly, A. M. El-Taher, T. R. Dalloul, Improved creep resistance and thermal behavior of Ni-doped Sn–3.0Ag–0.5Cu lead-free solder, J. Alloys Compd. 587 (2014) 32–39. https://doi.org/10.1016/j.jallcom.2013.10.148
[7] A. Singh, H. L. Choo, W. H. Tan, R. Durairaj, S. Janasekaran, M. S. Senthil Saravanan, A review: Effect of nanoparticle additions on the physical, microstructural, interfacial and mechanical properties of low temperature SnBi solder alloys, JOM 77 (2025) 4226–4245. https://doi.org/10.1007/s11837-025-07201-9
[8] F. Wang, H. Chen, Y. Huang, L. Liu, Z. Zhang, Recent progress on the development of Sn–Bi based low-temperature Pb-free solders, J. Mater. Sci. Mater. Electron. 30 (2019) 3222–3243. https://doi.org/10.1007/s10854-019-00701-w
[9] K. N. Tu, K. Zeng, Tin–lead (SnPb) solder reaction in flip chip technology, Mater. Sci. Eng. R. Rep. 34 (2001) 1–58. https://doi.org/10.1016/S0927-796X(01)00029-8
[10] Y. Li, W. Lin, X. Li, H. Ouyang, Effects of Zn contents on microstructure, thermodynamic characteristic and mechanical properties of Sn–Bi-based lead-free solder, J. Mater. Sci.: Mater. Electron. 33 (2022) 1741–1751. https://doi.org/10.1007/s10854-021-07153-1
[11] C.-B. Lee, S.-B. Jung, Y.-E. Shin, C.-C. Shur, The effect of Bi concentration on wettability of Cu substrate by Sn–Bi solders, Mater. Trans. 42 (2001) 751–755. https://doi.org/10.2320/matertrans.42.751
[12] S. Zhou, Y. Zhang, J. Duan, A. Yue, Y. Cao, Study on the preparation and properties of Sn–0.7Cu–xBi alloy, RSC Adv. 13 (2023) 35161–35171. https://doi.org/10.1039/D3RA06742D
[13] V. E. Sidorov, S. A. Uporov, D. A. Yagodin, K. I. Grushevskii, N. S. Uporova, D. V. Samokhvalov, Density, electrical resistivity and magnetic susceptibility of Sn-Bi alloys at high temperatures, High Temp. 50 (2012) 348–353. https://doi.org/10.1134/S0018151X12020174
[14] L. Zhang, K.N. Tu, Structure and properties of lead-free solders bearing micro and nano particles, Mater. Sci. Eng. R Rep. 82 (2014) 1–32. https://doi.org/10.1016/j.mser.2014.06.001
[15] S. Li, X. Wang, Z. Liu, Y. Jiu, S. Zhang, J. Geng, X. Chen, S. Wu, P. He, W. Long, Corrosion behavior of Sn-based lead-free solder alloys: a review, J. Mater. Sci.: Mater. Electron. (2020) 31 9076–9090. https://doi.org/10.1007/s10854-020-03540-2
[16] H. Ma, J. C. Suhling, A review of mechanical properties of lead-free solders for electronic packaging, J. Mater. Sci. 44 (2009) 1141–1158. https://doi.org/10.1007/s10853-008-3125-9
[17] Y.-A. Shen, Bi dispersion hardening in Sn-Bi Alloys by solid-state aging, JOM 75 (2023) 4922–4930. https://doi.org/10.1007/s11837-023-06079-9
[18] Y. Liu, H. Zhang, F. Sun, Solderability of SnBi-nano Cu solder pastes and microstructure of the solder joints, J. Mater. Sci.: Mater. Electron. 27 (2016) 2235–2241. https://doi.org/10.1007/s10854-015-4016-x
[19] W. Zhu, W. Zhang, W. Zhou, P. Wu, Improved microstructure and mechanical properties for SnBi solder alloy by addition of Cr powders, J. Alloys Compd. 789 (2019) 805–813. https://doi.org/10.1016/j.jallcom.2019.03.027
[20] M. S. Abdelaziz, H. Y. Zahran, A. F. Abd El-Rehim, Microstructure and mechanical properties of tin-bismuth solder alloy reinforced by antimony oxide nanoparticles, Int. J. Adv. Eng. Technol. 10 (2017) 73–83. http://www.dx.doi.org/10.5281/zenodo.3957492
[21] C. Thongchai, B. Lohwongwatana, C. Puncreobutr, A. Khamkongkaeo, T. Phetrattanarangsi, B. Sakkomolsri, P. Kidkhunthod, N. Chanlek, Study of microstructure and mechanical properties of commercially pure Sn and Sn-4 %Bi alloys fabricated by permanent mold gravity casting and forging, Eng. J. 22 (2018) 171–183. https://doi.org/10.4186/ej.2018.22.5.171
[22] B. Hu, W. Zhou, K. Tsuchiya, Effect of Bi additions on the microstructure evolution and surface instability during room-temperature aging of Sn alloys, J. Mater. Sci. 60 (2025) 11529–11547. https://doi.org/10.1007/s10853-025-11052-9
[23] W. Yang, W. Qin, J. Wu, J. Feng, Y. Zhan, Effect of graphene nanosheets on the microstructure and mechanical properties of Sn-20Bi solder, Mater. 16 (2023) 1550. https://doi.org/10.3390/ma16041550
[24] S. Amares, M. N. Ervina Efzan, R. Durairaj, A. Niakan, Influence of nano-3%Al_2O_3 on the properties of low temperature Sn-58Bi (SB) lead-free solder alloy, IOP Conf. Ser.: Mater. Sci. Eng. 205 (2017) 012002, https://doi.org/10.1088/1757-899X/205/1/012002
[25] L. Yang, J. Dai, Y. Zhang, Y. Jing, J. Ge, H. Liu, Influence of BaTiO3 nanoparticle addition on microstructure and mechanical properties of Sn-58Bi solder, J. Electron. Mater. 44 (2015) 2473–2478. https://doi.org/10.1007/s11664-015-3796-3
[26] H. Peng, X.-C. Lü, T.-S. Lin, H.-X. Li, J. An, X. Ma, J. Feng, Y. Zhang, Q. Li, Y. Qian, Improvement of mechanical properties of Sn–58Bi alloy with multi-walled carbon nanotubes, Trans. Nonferrous Met. Soc. China 22 (2012) s692–s696. https://doi.org/10.1016/S1003-6326(12)61788-9
[27] ASTM E384-22. Standard Test Method for Microindentation Hardness of Materials. ASTM International. Accessed 17 January 2026. https://store.astm.org/e0384-22.html
[28] P. Terek, D. Kukuruzović, L. Kovačević, A. Miletić, V. Terek, B. Škorić, P. Panjan, M. Čekada, The influence of CrAlN coating chemical composition on soldering resistance in contact with Al-Si-Cu alloy, Mater. Proc. 2 (2020) 28. https://doi.org/10.3390/CIWC2020-06837
[29] Z. Lai, D. Ye, Microstructure and fracture behavior of non-eutectic Sn–Bi solder alloys, J. Mater. Sci.: Mater. Electron. 27 (2016) 3182–3192. https://doi.org/10.1007/s10854-015-4143-4
[30] W. D. Callister Jr., Materials Science and Engineering: An Introduction, 3rd ed., John Wiley & Sons, 1994. ISBN: 978-1-118-47770-0
[31] X. Lv, Z. Pan, Y. Liu, C. Zhang, Z. Wang, F. Sun, Effects of Bi and In addition on microstructure and properties of Sn-0.7Cu solder, Metals 15 (2025) 157. https://doi.org/10.3390/met15020157

[32] X. F. Tan, Q. Hao, J. Zhou, S. D. McDonald, K. Sweatman, K. Nogita, The effect of temperature on the electrical resistivity of Sn-Bi alloys, J. Electron. Mater. 53 (2024) 1183–1191. https://doi.org/10.1007/s11664-023-10849-1

[33] Y. Plevachuk, V. Poverzhuk, P. Svec Sr., P. Svec, I. Janotová, D. Janickovic, A. Rud, Electrical resistivity of lead-free solders reinforced by carbon nanospheres, Int. J. Thermophys. 45 (2024) 31. https://doi.org/10.1007/s10765-023-03326-8

[34] S. M. L. Nai, J. Wei, M. Gupta, Effect of carbon nanotubes on the shear strength and electrical resistivity of a lead-free solder, J. Electron. Mater. 37 (2008) 515–522. https://doi.org/10.1007/s11664-008-0379-6

[35] P. Babaghorbani, S. M. L. Nai, M. Gupta, Reinforcements at nanometer length scale and the electrical resistivity of lead-free solders, J. Alloys Compd. 478 (2009) 458–461. https://doi.org/10.1016/j.jallcom.2008.11.074

[36] E. A. Eid, A. Fawzy, M. M. Mansour, G. Saad, M. Amin, Microstructural examination and thermodynamic analysis of Sn-1.5Ag-0.5Cu-x mass% Ni lead-free solder alloys, J. Therm. Anal. Calorim. 149 (2024) 4313–4331. https://doi.org/10.1007/s10973-024-13018-6

[37] Y. Altintas, Y. Kaygisiz, E. Öztürk, S. Aksöz, K. Keşlioğlu, N. Maraşli, The measurements of electrical and thermal conductivity variations with temperature and phonon component of the thermal conductivity in Sn–Cd–Sb, Sn–In–Cu, Sn–Ag–Bi and Sn–Bi–Zn alloys, Int. J. Therm. Sci. 100 (2016) 1–9. https://doi.org/10.1016/j.ijthermalsci.2015.09.004

[38] D. Wu, Z. Ning, Y. Zhu, R. Yuan, Evaluation of thermal and mechanical properties of Bi-In-Sn/WO_3 composites for efficient heat dissipation, Mater. 17 (2024) 5315. https://doi.org/10.3390/ma17215315

[39] M. M. Mousa, M. M. Mohammed, O. A. El-Kady, H. S. Mohamed. Microstructure, hardness, electrical, and thermal conductivity of SZCN solder reinforced with TiO_2 and ZrO_2 nanoparticles fabricated by powder metallurgy method, J. Mater. Sci.: Mater. Electron. 35 (2024) 1133. https://doi.org/10.1007/s10854-024-12758-3

[40] K. N. Božinović, D. M. Manasijević, L. T. Balanović, M. D. Gorgievski, U.S. Stamenković, M. S. Marković, Z.D. Mladenović, Study of microstructure, hardness and thermal properties of Sn-Bi alloys, Hem. Ind. 75 (2021) 227–239. https://doi.org/10.2298/HEMIND210119021B .

[41] T. M. Tritt. Thermal Conductivity: Theory, Properties, and Applications. Springer Science & Business Media, 2005. ISBN978-0-306-48327-1.

[42] N. Jiang, L. Zhang, Z.-Q. Liu, L. Sun, W.-M. Long, P. He, M.-Y. Xiong, M. Zhao, Reliability issues of lead-free solder joints in electronic devices, Sci. Technol. Adv. Mater. 20 (2019) 876–901. https://doi.org/10.1080/14686996.2019.1640072

[43] W. Firdaus, B. Soegijono, A. Sudarmadji, A. D. Trisnadi, Characterization of bismuth in Sn-based as safe environment solder material, AIP Conf. Proc. 2242 (2020) 020011. https://doi.org/10.1063/5.0007974

[44] S. N. Alam, N. Jindal, N. Naithani, Effect of addition of Cu on the properties of eutectic Sn-Bi solder alloy, Mater. Sci.-Pol. 37 (2019) 212–224. https://doi.org/10.2478/msp-2019-0032

[45] L. C. Tsao, S. Y. Chang, Effects of nano-TiO_2 additions on thermal analysis, microstructure and tensile properties of Sn3.5Ag0.25Cu solder, Mater. Des. 31 (2010) 990–993. https://doi.org/10.1016/j.matdes.2009.08.008